Can an External Electric Field Switch between Ethylene Formation and L-Arginine Hydroxylation in the Ethylene Forming Enzyme?

Shobhit S. Chaturvedi, ‡[a] Simahudeen Bathir Jaber Sathik Rifayee, ‡[a] Rajeev Ramanan,[b] Joel A. Rankin,[c] Jian Hu,[d,e] Robert P. Hausinger,[c,d] Christo Z. Christov[a,*]

[a] Department of Chemistry, Michigan Technological University, Houghton, MI 49931, USA.

[b] Department of Chemistry, National Institute of Technology, Rourkela, OR 769008, India.

[c] Department of Microbiology and Molecular Genetics, Michigan State University, East Lansing, MI 48824, USA.

[d] Department of Biochemistry and Molecular Biology, and [e] Department of Chemistry, Michigan State University, East Lansing, MI 48824, USA.

*Corresponding Author: Christo Z. Christov: christov@mtu.edu

‡ Authors with equal contribution.

Abstract

The non-heme Fe(II) and 2-oxoglutarate (2OG) dependent ethylene-forming enzyme (EFE) catalyzes both ethylene generation and L-Arg hydroxylation. Despite experimental and computational progress in understanding the mechanism of EFE, no EFE variant has been optimized for ethylene production while simultaneously reducing the L-Arg hydroxylation activity. In this study, we show that the two L-Arg binding conformations, associated with different reactivity preferences in EFE, lead to differences in the intrinsic electric field (IntEF) of

EFE. Importantly, we suggest that applying an external electric field (ExtEF) along the Fe-O bond in the EFE·Fe(III)·$OO^{\cdot-}$·2OG·L-Arg complex can switch the EFE reactivity between L-Arg hydroxylation and ethylene generation. Furthermore, we explored how applying an ExtEF alters the geometry, electronic structure of the key reaction intermediates, and the individual energy contributions of second coordination sphere (SCS) residues through combined quantum mechanics/molecular mechanics (QM/MM) calculations. Experimentally generated variant forms of EFE with alanine substituted for SCS residues responsible for stabilizing the key intermediates in the two reactions of EFE led to changes in enzyme activity, thus demonstrating the key role of these residues. Overall, the results of applying an ExtEF indicate that making the IntEF of EFE less negative and stabilizing the off-line binding of 2OG is predicted to increase ethylene generation while reducing L-Arg hydroxylation.

Introduction

Ethylene is among the most important organic chemicals and is an essential building block in the production of plastics, textiles, antifreeze, PVC pipes, tires, etc.[1,2] Ethylene also plays a vital role as a plant hormone, influencing their growth and development and initiating fruit ripening.[3] Industrial ethylene synthesis by the thermal cracking of natural gas and petroleum requires a high energy input, which involves burning fuels that release large quantities of greenhouse gases with consequent adverse effects on the environment.[4] Therefore, efforts have been directed toward finding new processes to produce ethylene without generating adverse environmental effects. Interestingly, certain bacteria and fungi can produce ethylene using the ethylene-forming enzyme (EFE).[5,6] Intensive investigations of EFE from *Pseudomonas syringae* strain PK2

demonstrate that it is a non-heme Fe(II) and 2-oxoglutarate (2OG) dependent enzyme that uses 2OG, dioxygen, and L-arginine (L-Arg) as substrates.[7–14] In the primary reaction, EFE catalyzes the decomposition of 2OG to generate ethylene plus two molecules of CO_2 and bicarbonate. The other reaction catalyzed by EFE is the oxidative decarboxylation of 2OG, forming succinate and CO_2, coupled with C5 hydroxylation of L-Arg to form a product that decomposes to guanidine and L-Δ^1-pyrroline-5-carboxylate (P5C).[10,11] Although enzyme catalysis by EFE releases CO_2 during the reaction, this level of CO_2 production is less than the amount of greenhouse gas released in the industrial processes, and it can be further reduced by expressing EFE in a cyanobacterium which allows for light-driven CO_2 fixation.[15–18]

Previous experimental and computational studies of the reaction mechanism of EFE have demonstrated that its two reactions diverge during the reaction of iron-bound superoxide with 2OG (Scheme 1).[12,19–21] As seen in other 2OG-dependent enzymes, the L-Arg hydroxylation pathway proceeds through an attack of superoxide on 2OG, leading to decarboxylation and forming a Fe(II)-succinyl-peroxide intermediate.[22–24] The Fe(II)-succinyl-peroxide intermediate rearranges to form succinate and a ferryl intermediate, which initiates L-Arg hydroxylation through hydrogen atom transfer (HAT) followed by rebound hydroxylation.[12] In contrast, the ethylene formation pathway involves dioxygen insertion into the C1-C2 bond of 2OG, leading to the formation of a computationally predicted and later experimentally trapped (bi)carbonate intermediate, which is exclusively linked to ethylene production by EFE.[13,19–21] Recent experiments suggested a radical coupling between the propanoate-3-yl and the Fe(III)-coordinated carbonate to generate 2-(1-carboxyethyl)carbonate, followed by a Grob-like fragmentation to produce ethylene (Scheme 1).[13] Despite all the experimental and

computational progress in establishing the ethylene-forming and L-Arg hydroxylation mechanisms of EFE, increasing ethylene production while reducing the hydroxylation reaction remains challenging. Multiple experiments to generate EFE variants showed that they either suppress or do not increase ethylene production while maintaining different levels of L-Arg hydroxylation reactivity.[7,8,12,14,25] Therefore, efforts toward identifying factors uniquely affecting the ethylene and L-Arg hydroxylation reactions in EFE (Scheme 1) are vitally important to guide the effective design of EFE variants with increased ethylene productivity.

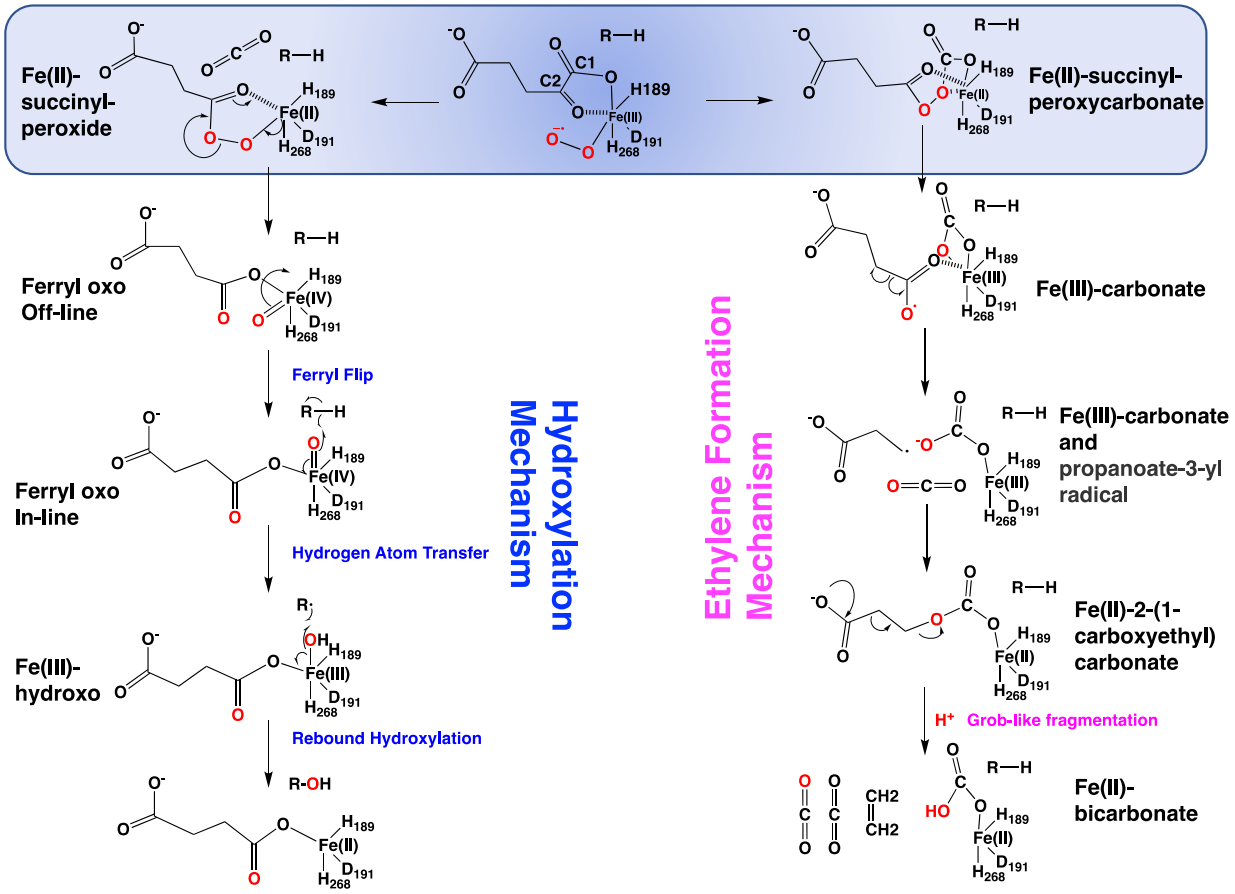

Scheme 1. Mechanisms and intermediates involved in the ethylene and L-Arg hydroxylation reactions of EFE. The diverging intermediates for the two reactions are highlighted. The residue numbers are obtained from the crystal structure geometry (PDB ID:5V2Y)[7].

A crystallographic study on EFE first demonstrated that the substrate L-Arg could exist in two conformations – A and B - which differ in the positioning of the guanidino group and the C5-methylene where the hydroxylation occurs.[8] In our previous published study,[20] we observed that these distinct positions affect the subsequent reactions of the enzyme by using a long time scale (1 μs) molecular dynamics and QM/MM calculations on wild-type (WT) EFE. Even though the molecular dynamics simulations were started using the L-Arg conformation A,[7] the simulations predicted the conformational transition and some stability of L-Arg conformation B. Moreover, the results indicated that nearby second coordination interactions were affected by a change in L-Arg conformation. For example, the crucial stabilization of the C1 carboxylate of 2OG by R171, which leads to the formation of the bicarbonate intermediate, is better in L-Arg conformation B than in L-Arg conformation A. Our calculations on WT EFE supported the hypothesis that, with off-line bound 2OG (i.e., a conformation of 2OG that positions the oxygen binding site such that it does not point toward the L-Arg substrate, Scheme 1), the L-Arg conformation A favors the L-Arg hydroxylation reaction, and L-Arg conformation B favors the formation of ethylene.[20] To date, there is no experimental evidence to indicate the formation of an in-line EFE·Fe(III)·$OO^{\cdot-}$·2OG·L-Arg complex in EFE (i.e., a 2OG conformation that causes the bound superoxide to point toward L-Arg). The QM/MM studies on WT EFE also indicate that off-line binding of 2OG is preferred in EFE as the transformation from off-line to in-line 2OG is energetically costly (21.8 kcal/mol)[20] in contrast to the same process in histone demethylase PHF8 (1.4 kcal/mol)[26] and DNA demethylase AlkBH2 (2.9 kcal/mol).[27] However, if in-line 2OG coordination is stabilized to exist in EFE, this conformation was predicted to only lead to hydroxylation regardless of the L-Arg conformation.[20]

Xue et al. indicated that the intrinsic electric field (IntEF) generated by the EFE protein scaffold promotes the formation of the Fe(II)-succinyl-peroxy carbonate intermediate, ultimately leading to ethylene formation in EFE.[19] Along these lines, multiple studies have predicted the importance of electrostatic effects in enzyme catalysis.[28–37] Extending this notion, Shaik and co-workers have even utilized external electric fields (ExtEF) on several small model complexes and enzymes to improve their reaction efficiencies and selectivities.[38–42] A computational study predicted that an ExtEF applied along the reaction axis of Diels-Alder reactions can catalyze/inhibit the rate and control its endo/exo selectivity;[43] this prediction was validated by Coote and colleagues in an experimental setup.[44] Recently, the role of an IntEF on the reactivity of a very similar 2OG-dependent enzyme, TET2, has been revealed.[45] Applying an ExtEF to the non-heme 2OG-dependent KDM4E enzyme was demonstrated to promote HAT from the C-H group of the methylated arginine substrate.[46] Several computational and experimental reports have proposed that the IntEF of an enzyme provides a preorganized polar environment that stabilizes the transition state (TS) during enzyme catalysis and influences the mechanistic crossover in several enzymes and small molecule reactions.[31,32,47–51]

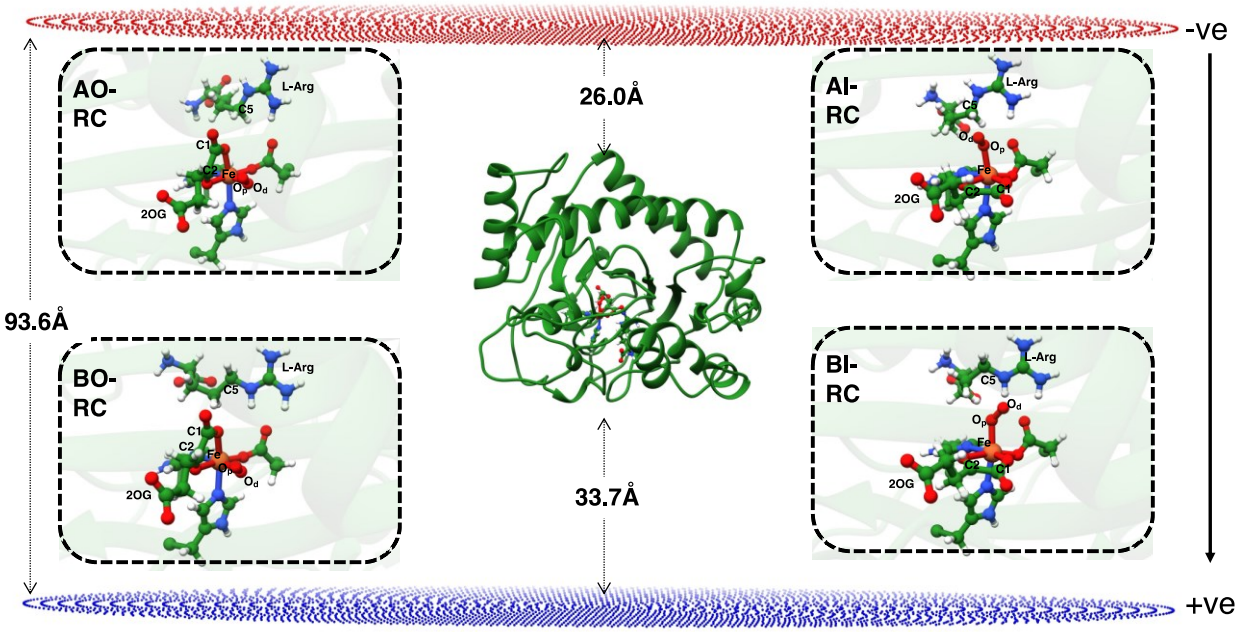

Figure 1. Two oppositely charged circular plates created with TITAN code are used to generate a uniform ExtEF on EFE. The negative charge plate is shown in red color, and the positive charge plate is shown in blue color. The direction of the ExtEF is along the Fe-O bond in all cases. The inset figures show the EFE·Fe(III)·$OO^{\cdot-}$·2OG·L-Arg complex with different 2OG and L-Arg conformations. The QM region is shown in balls and sticks.

In this study, we show that the IntEF along the Fe-O bond of EFE is predicted to differ between the 2OG/L-Arg binding modes that favor ethylene generation or L-Arg hydroxylation reactions. We indicate that by applying an ExtEF along the Fe-O bond in the EFE·Fe(III)·$OO^{\cdot-}$ ·2OG·L-Arg complex (Figure 1), we can switch between the two reaction mechanisms of EFE – ethylene formation and L-Arg hydroxylation. Furthermore, we elucidate the structural, electronic, and energetic characteristics of key reaction intermediates for both reactions and the

individual energetic contributions of EFE residues that are involved in stabilizing reaction-specific intermediates. We performed experimental studies in which key second coordination sphere (SCS) residues that stabilize the key intermediates (IMs) of the two EFE reactions were substituted with alanine; kinetic studies on several of these variants revealed changes in EFE activity. The results provide mechanistic suggestions on how to switch between the ethylene and L-Arg hydroxylation reactivity of EFE.

Methods

System Preparation:

A crystal structure of EFE in complex with L-Arg, 2OG, and Mn, an analog of Fe (PDB ID: 5V2Y)[7] was obtained from the RCSB protein data bank.[52] The Mn ion in the crystal structure is modified to iron (Fe) with an O_2 bonded end-on using Gauss View.[53] The Fe ion is ligated to two histidines (H189 and H268) and one aspartate (D191) (all monodentate). In the case of EFE.FE(III)-$OO^{\bullet-}$.$2OG_{off\text{-}line}$.L-Arg complex, 2OG was in off-line bidentate coordination with Fe. Hydrogens were added to the ionizable side chains of the protein based on their local environment using the Chimera tool.[54] The topology for 2OG and O2 was obtained using the GAFF tool in Antechamber.[55] The Fe(III) center parameters in its high-spin (HS) state (S=2, M=5) were obtained using Metal Center Parameter builder (MCPB.py v3.0).[56] The force constant values for bonds and angles in MCPB were derived at the B3LYP/6-31G* level of theory. The remaining portion of the protein is modeled using the Amber FF14SB force field.[57] The same procedure is used to derive parameters for the EFE.FE(III)-$OO^{\bullet-}$.$2OG_{in\text{-}line}$.L-Arg complex, where 2OG is bound with in-line bidentate

coordination to Fe. The protein systems are then solvated using TIP3P water molecules up to 10 Å from the farthest protein boundary and neutralized with counter ions (Na^+) using the leap module in Amber 16. The systems obtained were used for MD simulations.

MD Simulations:

The MD simulations of the prepared systems were performed in the GPU version of the Amber 16 package.[58] Periodic boundary conditions were employed in all the simulations. Initial minimization of the systems involves relaxing only the solvent to remove bad water contact with the enzyme by applying a restraint of 100 kcal mol^{-1} on the enzyme. The second minimization involves relaxing the whole system, including the enzyme. In each of the above steps, the system is minimized by 5000 steps of the steepest descent and 5000 steps of the conjugate gradient methods. The system was then heated gently from 0 to 300k under NVT ensemble using a Langevin thermostat[59] with a collision frequency of 1 ps^{-1} for 250ps with a small restraint of 50 kcal/mol on the enzyme. Further, the system is normalized under the NPT ensemble for 1 ns at a temperature of 300 K and pressure of 1.0 atm using the Langevin thermostat and Berendsen barostat,[60] respectively. Following that, the system is equilibrated for 3ns under the same conditions. A production simulation of 1000 ns with a timestep of 2 fs was carried out from the equilibrated structure under an NPT ensemble with a target pressure of 1 bar and constant pressure coupling of 2ps. SHAKE[61] and Particle Mesh Ewald[62] algorithms were used to constrain the hydrogen bonds and calculate the long-range electrostatic forces, respectively.

QM/MM Setup:

The starting QM/MM optimized structures of four EFE·Fe(III)·$OO^{\cdot-}$·2OG·L-Arg complexes were taken from two MDs of two systems using combinations of two L-Arg and 2OG conformations: (a) L-Arg A and Off-line 2OG (**AO**), (b) L-Arg B and Off-line 2OG (**BO**), (c) L-Arg A and In-line 2OG (**AI**), and (d) L-Arg B and In-line 2OG (**BI**). The WT EFE calculations for all the above snapshots were already reported in our previous work.[20] The IntEF measurements and the ExtEF plate generation along the Fe-O bond were done with TITAN (Figure S1).[63] The distance between the electric field plates is 93.6 Å, and between the plates and the surface of the enzyme is 26 and 33.7 Å from top and bottom, respectively. The protein retained a water solvation layer maximum of 12 Å from the protein surface. All water molecules further away from 12 Å from the protein were truncated. The QM/MM calculations under ExtEFs were performed using ChemShell,[64] combining TURBOMOLE[65] for the QM part and DL_POLY[66] for the MM part. The setup for the QM/MM calculations was kept the same as for the WT EFE calculations[20] as the computational predictions from the WT study were validated by an experimental study on EFE.[13] The non-heme Fe, the coordinating residues (H189, D191, and H268), 2OG, dioxygen, and the substrate L-Arg were included in the QM region (Figure 1). The calculations were performed at the ground state (quintet spin state, *S*=2) of non-heme Fe enzymes.[67] The unrestricted B3LYP functional[68] was used to represent the QM region as it has been used to accurately model the reaction mechanism in studies of the WT EFE[19–21] and several similar 2OG-dependent enzymes.[26,45,69–72] All protein and water atoms beyond the QM region were included in the MM region, and the Amber FF14SB force field was used to represent them.[57] The flexible region was allowed to change its coordinates during optimizations and includes the QM part plus all the MM atoms within 8 Å

from the QM part. The remaining part of the system (MM atoms which are further away than 8 Å from the QM part) was kept fixed. Although a study demonstrated that usually moving atoms further than 6 Å from the QM part should not considerably influence the quality of the calculations,[73] we should be cautious about the potential effects of not optimizing a larger region, for example, such as differences in the geometries and energies of the optimized structures, and different orientations of the SCS residues among others. QM/MM boundaries were capped with a hydrogen link atom, and the effect of MM polarization on the QM region was accounted for using an electrostatic embedding scheme.[74] Geometry optimizations were performed with the def2-SVP [QM(B1)/MM] basis set.[75] From the QM/MM optimized reactant complexes in the presence of an ExtEF, transition states were searched along the reaction coordinate by a relaxed potential energy scan of step size 0.1 Å. The reaction coordinate tracked the decrease in distance of O_d (the distal atom of bound oxygen), the C_2 carbon of 2OG, and the increase in distance of the O_p-O_d bond. The potential energy surface (PES) plots of the adiabatic scans of all the systems are given in the SI (Figure S8-S11). In order to test the choice of the RC and explore the PES comprehensively, we also performed a test 2D PES calculation. The first dimension was defined by the decrease in the distance between C_2 and O_p(rc1), and the second dimension explored the increase in the distance between O_p and O_d(rc2). More details about the 2D PES calculations are presented in the SI (Pages S12-S15). The highest energy structure from the adiabatic scan was optimized using the DL-Find optimizer without any restraints.[76] The single-point energies were calculated to improve the energies using the large all-electron def2-TZVP[75] [QM(B2)/MM] basis set. The zero-point energy calculations were performed for all geometries, and all final energies in the manuscript are reported at the [QM(B2+ZPE)/MM] level of theory. Based on the nature of

the intermediate formed, the reaction specificity was determined, i.e., the Fe(II)-succinyl-peroxide intermediate and the Fe(II)-succinyl-peroxy carbonate intermediate were used as indicators for the L-Arg hydroxylation and ethylene reaction preference respectively.[13] The energy decomposition analysis (EDA) was performed using a Fortran90 program developed by the Cisneros research group.[77,78]

Biological studies included site-directed mutagenesis, protein purification, and assays for the production of ethylene and P5C. Several variant proteins were previously described,[7] but three new variants were investigated using modified methods. More details are presented in the SI.

Results and Discussions

Does the IntEF change in the different conformations of 2OG and L-Arg?

We first calculated the IntEF along the Fe-O bond in the six reported reactant complexes (RC) with different L-Arg conformations and 2OG binding modes that led to L-Arg hydroxylation and ethylene formation from our previous EFE calculations.[20] The two RC structures containing L-Arg in conformation A and off-line coordination of 2OG (**AO-RC**), leading to hydroxylation of L-Arg, have IntEF values along the Fe-O bond of -0.0333 and -0.0346 atomic units (au), respectively. Two other RC structures with L-Arg in conformation B and off-line coordination of 2OG (**BO-RC**), producing ethylene, have IntEF values of -0.0317 and -0.0319 au. Similarly, the snapshot with L-Arg in conformation A and in-line coordination of 2OG (**AI-RC**) has an IntEF value of -0.0352 au. In comparison, the RC with L-Arg in conformation B and in-line coordination of 2OG (**BI-RC**) has an IntEF of -0.0296 au. The IntEF analysis suggests that L-Arg conformation B, associated with

ethylene generation where 2OG is bound off-line, leads to less negative IntEF along the Fe-O bond in EFE compared to the L-Arg conformation A that is linked to the hydroxylation reaction.

Can an ExtEF switch the ethylene and L-Arg hydroxylation reaction mechanisms of EFE?

With no ExtEF applied, the **AO** conformation of EFE favors the L-Arg hydroxylation reaction pathway (**AO-RC-noExtEF**).[20] We tested whether applying positive ExtEFs with different intensities (+0.0025, +0.0050, +0.0075, and +0.010 au) or negative ExtEF (-0.0025, -0.0050, -0.0075 and -0.010 au) along the Fe-O bond in **AO-RC** will change its reactivity from L-Arg hydroxylation to ethylene formation (Figure 2). Indeed, the QM/MM reaction path calculations, starting from **AO-RC** under the influence of all four positive ExtEFs, show that the **AO** reactivity is predicted to switch to ethylene. The reaction now leads to the formation of a Fe(II)-succinyl-peroxy-carbonate intermediate (key intermediate for ethylene formation)[13] instead of a Fe(II)-succinyl-peroxide intermediate seen in **AO-RC-noExtEF** (that leads to L-Arg hydroxylation).[13] The ethylene-forming reactions are calculated to proceed with energy barriers between 8.5 and 9.8 kcal/mol at the different positive ExtEFs. The QM/MM calculations under the influence of negative electric fields of -0.0025 and -0.0050 au show the formation of a Fe(II)-succinyl-peroxide intermediate, indicating that the L-Arg hydroxylation reaction pathway is preferred. The reactions are calculated to proceed with energy barriers of 9.8 and 10.5 kcal/mol for the **AO-RC-0.0025** and **AO-RC-0.0050** snapshots with respect to 11.4 kcal/mol in **AO-RC-noExtEF**.[20] However, a further change of ExtEF to values of -0.0075 and -0.010 au is predicted to switch the reactivity of **AO** from L-Arg hydroxylation to ethylene formation. The Fe(II)-succinyl-peroxy carbonate intermediate formation in the **AO-RC-0.0075** and **AO-RC-0.010** snapshots are predicted to

proceed with energy barriers of 8.8 and 5.8 kcal/mol, respectively. The spin densities and charges for all stationary points are provided in the SI (Table S1-S16*). Thus, the QM/MM calculations of applying an ExtEF on* ***AO-RC*** *indicate that all magnitudes of a positive ExtEF and negative values of 0.075 and 0.010 au along the Fe-O bond are predicted to switch the catalyzed reaction selectivity from L-Arg hydroxylation to ethylene formation.*

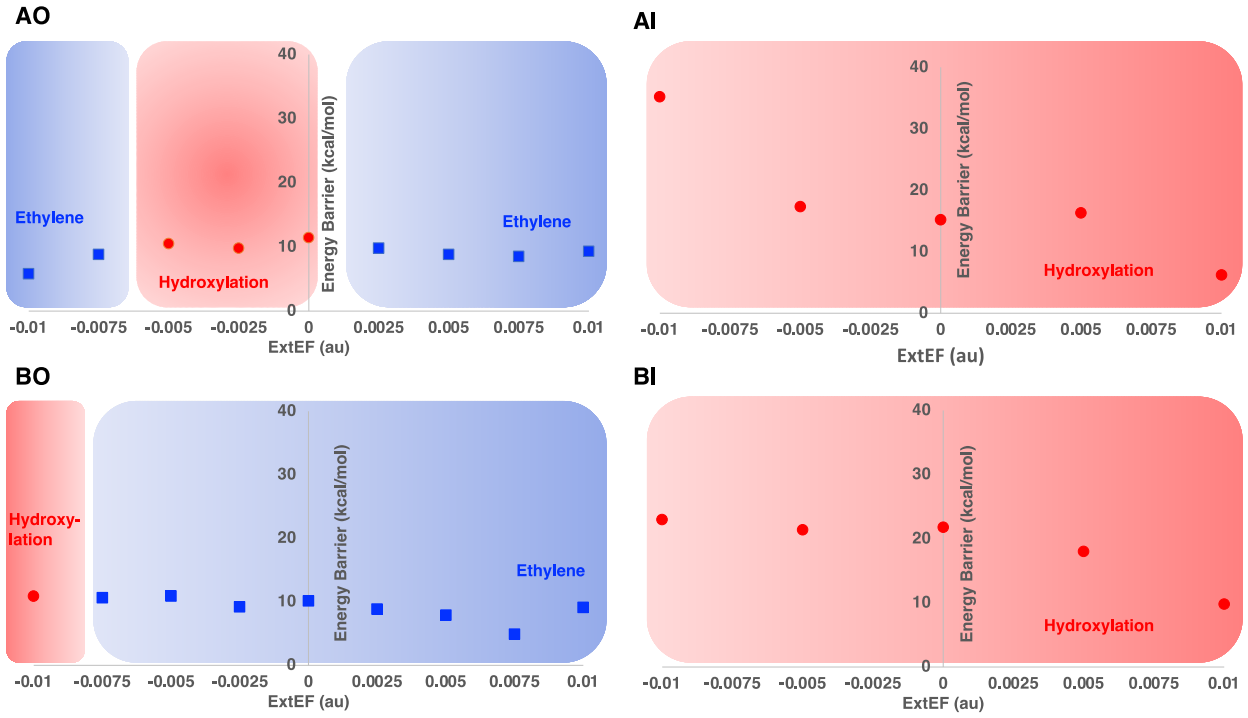

Figure 2. Reaction selectivities and energy barriers with respect to the strength of applied ExtEF along the Fe-O bond for different 2OG and L-Arg conformations of EFE – AO, BO, AI, and BI. The applied ExtEF is measured in atomic units (au). ExtEF with zero au corresponds to the WT EFE without any applied ExtEF.

The **BO-RC** leads to ethylene formation without an ExtEF (**BO-RC-noExtEF**).[20] The QM/MM calculations with positive electric fields of +0.0025, +0.0050, +0.0075, and +0.010 au, along the

Fe-O bond, show that **BO-RC** is predicted to retain its preference for the ethylene formation (Figure 2). The Fe(II)-succinyl-peroxy carbonate intermediate is created with energy barriers of 8.8, 7.9, 4.9, and 9.1 kcal/mol, respectively, in **BO-RC+0.0025**, **BO-RC+0.0050**, **BO-RC+0.0075**, and **BO-RC+0.010** reaction calculations. The energy barriers decrease with an increase of the ExtEF strength in BO-RC complexes until the ExtEF of +0.010 au, when the barrier rapidly increases. The basis of this interesting trend is unclear and requires further exploration. We might speculate that after a particular threshold, i.e., after ExtEF of +0.0075, additional effects quickly became dominant. When applying negative ExtEFs of -0.0025, -0.0050, and -0.0075 au on **BO-RC**, there is no predicted change in reaction specificity. However, increasing the intensity of a negative ExtEF to -0.010 au is calculated to switch the **BO-RC** reaction specificity from ethylene formation to L-Arg hydroxylation. The Fe(II)succinyl-peroxy carbonate intermediate is generated with an energy barrier of 9.2, 10.9, and 10.6 kcal/mol in **BO-RC-0.0025**, **BO-RC-0.0050**, and **BO-RC-0.0075**. For comparison, the Fe(II)-succinyl-peroxide intermediate in **BO-RC-0.010** requires a 10.9 kcal/mol energy barrier. The spin densities and charges for all stationary points are provided in the SI (Table S17-S32). *Thus, applying a positive ExtEF to **BO-RC** is predicted to maintain the reaction preference towards the ethylene reaction, while applying a strong negative electric field with a value of -0.010 au could change the reaction selectivity towards L-Arg hydroxylation.*

To date, there is no experimental evidence to indicate the formation of an in-line EFE·Fe(III)·OO·¯2OG·L-Arg complex in EFE, and QM/MM studies on WT EFE have also indicated that off-line binding of 2OG is favored. Nevertheless, we wanted to explore the effects of ExtEF on the in-line EFE·Fe(III)·OO·¯2OG·L-Arg complex from a theoretical/enzyme engineering

perspective. If EFE can be modified to stabilize an in-line binding of 2OG, we wondered if it could produce ethylene under the influence of external electric fields. The previous QM/MM calculations on the **AI** and **BI** RCs of WT EFE show that both RC conformations lead to L-Arg hydroxylation without an ExtEF.[20] We applied two positive electric fields of +0.0050 and +0.010 au and two negative electric fields of -0.0050 and -0.010 au on **AI-RC** and **BI-RC** to test if their reaction paths can be changed toward the ethylene formation. The QM/MM calculations of the four ExtEFs (+0.0050, +0.010, -0.050, and -0.010 au) on the **AI-RC** and **BI-RC** showed that both species are predicted to still lead to the formation of the Fe(II)-succinyl-peroxide intermediate, indicating the reaction selectivity for L-Arg hydroxylation is maintained (Figure 2). However, applying an ExtEF along the Fe-O bond in **AI** and **BI** conformations shows a trend in the calculated activation energy required for the decarboxylation reaction to form the Fe(II)-succinyl-peroxide intermediate. In the **AI** conformation, the energy barriers are 35.2, 17.3, 16.3, and 6.2 kcal/mol upon applying ExtEFs of -0.010, -0.050, +0.0050, and +0.010 au, respectively, in comparison to 15.2 kcal/mol without an ExtEF. Similarly, for the **BI** conformation, the energy barriers were 23.0, 21.4, 18.0, and 9.8 kcal/mol upon applying ExtEFs of -0.010, -0.050, +0.0050, and +0.010 au, respectively, in comparison to 21.8 kcal/mol without an ExtEF (Figure 2). The spin densities and charges for all stationary points are provided in the SI (Table S33-S48). *Thus, the results of calculations using positive and negative ExtEFs indicate that the electrostatic effects created by ExtEFs do not influence the reaction selectivity when the 2OG is in-line coordinated to Fe, irrespective of the L-Arg conformation. However, ExtEFs are predicted to modulate the activation energy of the O_2 activation mechanism step in the L-Arg hydroxylation reaction.*

To further validate the results, we have included additional calculations with an expanded QM region and tested if applying an external electric field changes the spin state reactivity preference of the EFE·Fe(III)·$OO^{\cdot-}$ complex. The expanded QM calculations included the two salt bridges formed between the 2OG C1 carboxylate and R171 and the 2OG C5 carboxylate and R277, and these computations were performed on the **AO+0.0025** structure that first switched towards L-Arg hydroxylation from ethylene (Figure S2). The calculations on the **AO+0.0025** structure with an expanded QM region show a transition state energy barrier of 10.8 kcal/mol at the [QM(B1+ZPE)/MM] level of theory compared to a barrier of 8.8 kcal/mol for the smaller QM region calculation at the same level of theory. The calculations reproduced the results of smaller QM region calculations with small differences in the geometries and activation energy, suggesting that the currently used QM region represents the key chemical changes in the system. To investigate the effect of applying an external electric field on the spin state reactivities of the EFE·Fe(III)·$OO^{\cdot-}$ complex, we performed additional calculations with septet and triplet spin states on the **AO+0.0025** structure (that first switched towards ethylene from L-Arg hydroxylation). The calculations show that the triplet **AO-RC+0.0025** is higher in energy by 11.7 kcal/mol, while the septet **AO-RC+0.0025** is slightly lower in energy by -1.9 kcal/mol in comparison to the quintet **AO-RC+0.0025**. However, both the septet and triplet spin state calculations show larger activation barriers of 15.1 and 37.8 kcal/mol compared to the quintet spin state barrier of 7.9 kcal/mol. These calculations performed under an ExtEF are in agreement with the quintet spin state preference in WT EFE without an ExtEF[19] and with other 2OG-dependent oxygenases without an ExtEF.[69,72,79,80] *It is important to note that a reordering of the spin states upon*

imposing an ExtEF could not be entirely excluded; however, the answer to this question would require additional calculations.

How does the ExtEF influence the geometric and electronic structure of the RCs?

The change of reaction specificity from hydroxylation to ethylene formation in the **AO** conformation happens at an ExtEF value of +0.0025 au. Therefore, we explored the changes in the geometric and the electronic structure properties of the QM/MM optimized EFE·Fe(III)·$OO^{\cdot-}$·2OG·L-Arg intermediate at an ExtEF of +0.0025 au (**AO-RC+0.0025**) with respect to the same QM/MM optimized structure without any ExtEF (**AO-RC-noExtEF**) (Figure 3).[20] An ExtEF of +0.0025 au is predicted to lead to a slight reduction in the Fe-O bond length from 2.09 Å in **AO-RC-noExtEF** to 2.06 Å in **AO-RC+0.0025**. The ExtEF also slightly affects the distance between the distal oxygen (Od) of the superoxo complex and C2 of 2OG (2.38 Å in **AO-RC+0.0025** compared to 2.33 Å in **AO-RC-noExtEF**) (Figure S3).[20] The spin densities on Fe, Od, and the proximal oxygen (Op) are calculated to undergo very slight reductions from 4.19, -0.24, and -0.49, respectively, in **AO-RC-noExtEF**[20] to 4.18, -0.21, -0.48 in **AO-RC+0.0025** (Table S1).

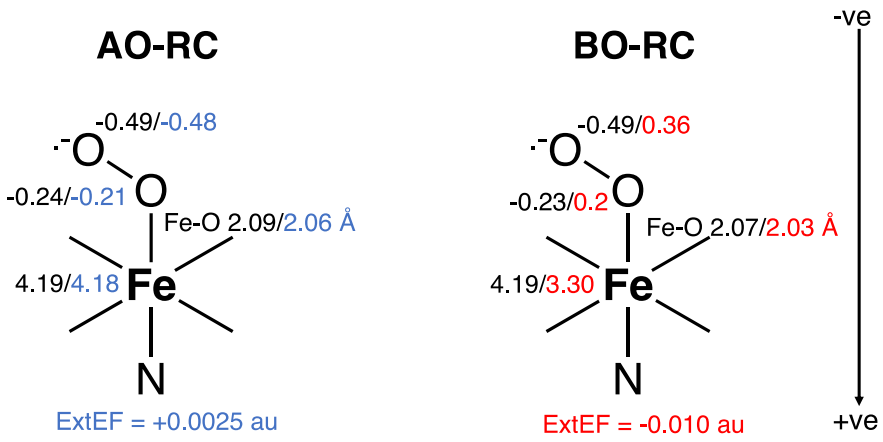

Figure 3. Spin density and Fe-O bond length variations as the ExtEF switches the reaction preference. The values for the WT system, the AO-RC sample with an ExtEF+0.0025 au, and the BO-RC sample with an ExtEF-0.010 au are given in black, blue, and red, respectively.

For the EFE **BO** conformation, switching the reaction selectivity from ethylene formation to L-Arg hydroxylation is predicted to occur at an ExtEF value of +0.010 au. The Fe-O bond length is calculated to be reduced in **BO-RC-0.010** to 2.03 Å from the 2.07 Å in **BO-RC-noExtEF**. The distance between Od and C2 of 2OG is computed to increase to 2.71 Å in **BO-RC-0.010** from the 2.32 Å in **BO-RC-noExtEF** (Figure S3).[20] The unpaired spin density on Fe reduces to 3.30 in **BO-RC-0.010** (Table S31) compared to 4.19 in **BO-RC-noExtEF**.[20] Additionally, the unpaired electron densities on Op and Od are reversed from the negative spin density values of -0.23 and -0.49 in **BO-RC-noExtEF**[20] to the positive spin density values of 0.20 and 0.36 in **BO-RC-0.010** (Table S31). *Thus, the computational results indicate the ExtEF leads to fine changes in the spin densities of Fe and O_2 and affects the Fe-O bond and Od-C2 distances.*

Effect of ExtEFs on the key Fe-O bonding orbitals of the RCs

The Fe-O bonding in **AO-RC-noExtEF**, which leads to L-Arg hydroxylation, results from the coupling between the Fe d_{xz} and the O_2 $\pi^*_{\perp}$ orbitals.[20] In **BO-RC-noExtEF** (which leads to ethylene production), the Fe-O bonding results from the coupling between the Fe $d_{x^2-y^2}$ and the O_2 $\pi^*_{||}$ orbitals.[20] In contrast to **BO-RC-noExtEF** and similarly to **AO-RC-noExtEF**, the Fe-O bonding in **AO-RC+0.0025**, for ExtEF-induced ethylene generation, results from the coupling between the Fe d_{xz} and the O_2 $\pi^*_{\perp}$ orbitals (Figure 4). In contrast, the calculated Fe-O bonding in the ExtEF-induced L-Arg hydroxylation pathway **BO-RC-0.010** is similar to that in the WT L-Arg hydroxylation

pathway (**AO-RC-noExtEF**);[20] i.e., orbitals in both cases result from the coupling between the Fe d_{xz} with the dioxygen $\pi^*_{\perp}$ orbitals. *The results indicate that the ExtEF can alter the occupancy of the β electron between the $\pi^*_{//}$ and $\pi^*_{\perp}$ dioxygen orbitals. Furthermore, the analysis of the EFE reactivities with and without ExtEF*[20] *indicates the ethylene-forming reaction mechanism can proceed using a molecular orbital (MO) derived from the combination of a Fe d-orbital (d_{xz} or $d_{x^2-y^2}$) with either the dioxygen $\pi^*_{//}$ or $\pi^*_{\perp}$ orbitals. However, the L-Arg hydroxylation reaction in EFE is predicted to proceed only through the participation of the MO that results from the overlap between the Fe d_{xz} with the dioxygen $\pi^*_{\perp}$ orbitals.*

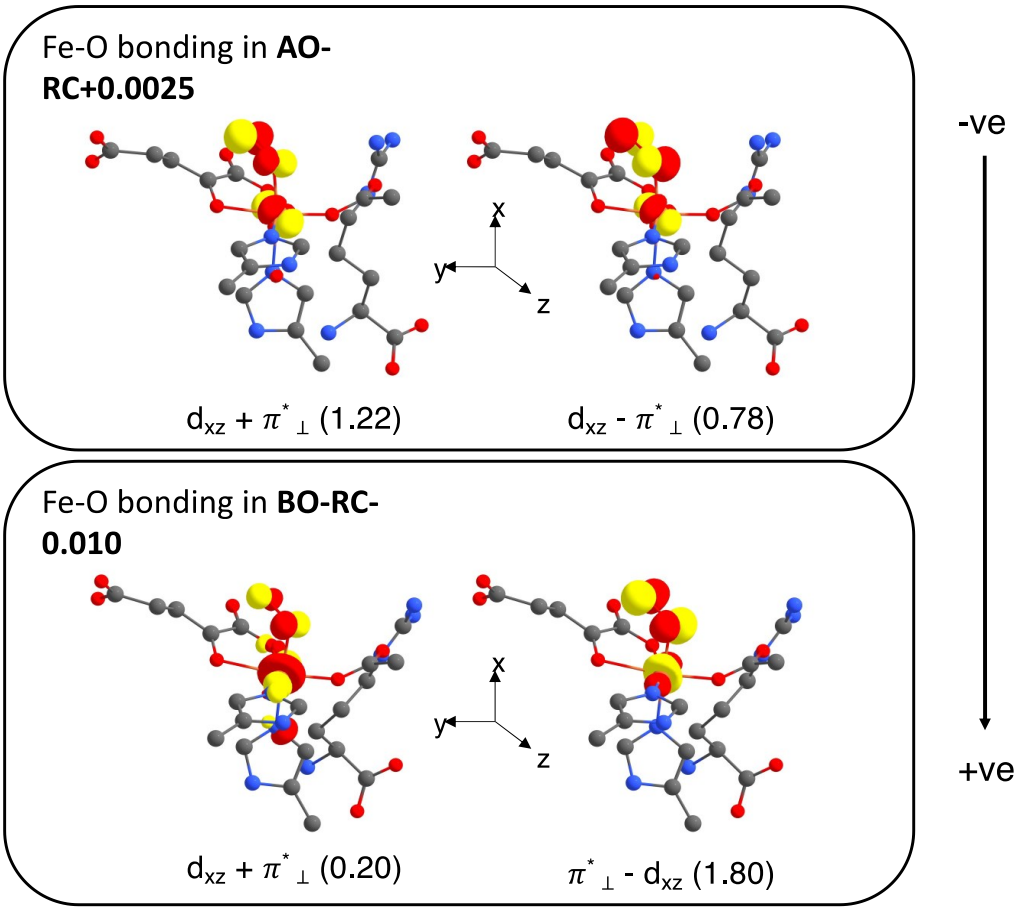

Figure 4. The Fe-O bonding natural orbitals (NOs) and their occupation numbers as the ExtEF values switch the reaction preference from L-Arg hydroxylation to ethylene production in **AO-RC+0.0025** and from ethylene generation to L-Arg hydroxylation in **BO-RC-0.010**. The direction of the ExtEF is depicted by the arrow.

Additionally, applying a positive ExtEF along the Fe-O bond is calculated to lead to a movement of electron density from the dioxygen-based $d_{xz} - \pi^*_{\perp}$ orbital to the Fe-based $d_{xz} + \pi^*_{\perp}$ orbital. This shift is indicated by the increase in natural orbital (NO) occupation numbers from 1.20 in **AO-RC-noExtEF**[20] to 1.22 in **AO-RC+0.0025** for the Fe-based $d_{xz} + \pi^*_{\perp}$ orbital (Figure 4 and Table S49) and reduction from 0.80 in **AO-RC-noExtEF**[20] to 0.78 in **AO-RC+0.0025** for the dioxygen-based $d_{xz} - \pi^*_{\perp}$ orbital. This trend is maintained as the intensity of the positive ExtEF is increased (Table S49). In contrast, applying a negative ExtEF is calculated to lead to electron movement from the Fe-based $d_{xz} + \pi^*_{\perp}$ orbital to the dioxygen-based $d_{xz} - \pi^*_{\perp}$ orbital. The NO occupation number is decreased to 0.20 in **BO-RC-0.010** for Fe-based $d_{xz} + \pi^*_{\perp}$ orbital from 1.22 in **BO-RC-noExtEF**,[20] and it increases to 1.80 in **BO-RC-0.010** for the dioxygen-based $d_{xz} - \pi^*_{\perp}$ orbital from 0.78 in **BO-RC-noExtEF**.[20] The same trend is sustained as the intensity of the negative ExtEF is increased (Table S49). *Thus, applying positive ExtEFs is predicted to lead to a slight movement of electron density from the dioxygen-based orbital to the Fe-based orbital, and the opposite movement is observed from the Fe-based orbital to the dioxygen-based orbital when applying negative ExtEFs.*

Are ExtEF-induced changes in the individual energetic contributions from SCS residues responsible for switching between the competing reactions?

We further analyzed whether the ExtEFs lead to changes in the nature of the SCS residues that energetically stabilize the respective intermediates leading to either L-Arg hydroxylation or ethylene production. For this aim, we performed EDA on the QM/MM optimized structures of the respective RCs and IMs. For the **AO** snapshot, which favors the L-Arg hydroxylation reaction in the absence of an ExtEF, the analysis indicates that R184 (-3.59 kcal/mol), E285 (-1.88), and K269 (-1.54) are among the primary residues contributing to the stabilization of the Fe(II)-succinyl-peroxide intermediate with respect to the reactant complex (Figure S4). Residues E84 (8.27), D91 (7.11), and R171 (5.90) are the primary side chains contributing to the destabilization of the Fe(II)-succinyl-peroxide intermediate (Figure S4). We then performed EDA on the QM/MM optimized EFE **BO-RC** structures, which led to ethylene production without any ExtEF. Residues R171 (-1.31) and D253 (-0.82) are the primary intermediate stabilizing residues, while E84 (1.79), D91 (1.01), and R277 (0.34) are the primary intermediate destabilizing residues with respect to the reactant complex (Figure S5). R171 stabilizes 2OG binding through hydrogen bonding interactions with the C1 carboxylate.[7,8,20] R171 also makes a π-π stacking interaction with the substrate L-Arg.[7,20] E84 is present in the L-Arg substrate binding pocket and makes a hydrogen bonding interaction with R171. D91 makes a hydrogen bonding interaction with L-Arg, and R184 makes a hydrogen bonding interaction with D91 to stabilize its orientation for interaction with L-Arg. D253, E285, and K269 are located near the surface and might affect the EFE activities through longer-range interactions. The importance of several of these residues has been experimentally demonstrated by prior site-directed mutagenesis studies,[7] and extended to the full list of

residues here (Table S50). In all cases, alanine was used for the substitutions to maintain uniformity. For example, E84A, D91A, R171A, D253A, and E285A variants of EFE lost essentially all capacity to form ethylene and exhibited greatly reduced L-Arg hydroxylation activity. In contrast, the R184A and K269A variants of EFE retained more than half of their ethylene formation and L-Arg hydroxylation activities.[7] Computer simulations are in progress to identify favorable substitutions to replicate the effect of ExtEF and to be further experimentally validated in future studies. The overall EDA results indicate that the Fe(II)-succinyl-peroxide intermediate in **AO-noExtEF**, used for L-Arg hydroxylation, prefers higher magnitudes of individual energetic contributions, e.g., 8.27 from E84, 7.11 from D91, 5.90 from R171, and -3.59 from R184 (Figure S4). In contrast, the Fe(II)-succinyl-peroxycarbonate intermediate in **BO-noExtEF** favors lower magnitude residue energetic contributions, e.g., 1.79 from E84, 1.01 from D91, -1.31 from R171, and -0.82 from D253 (Figure S5).

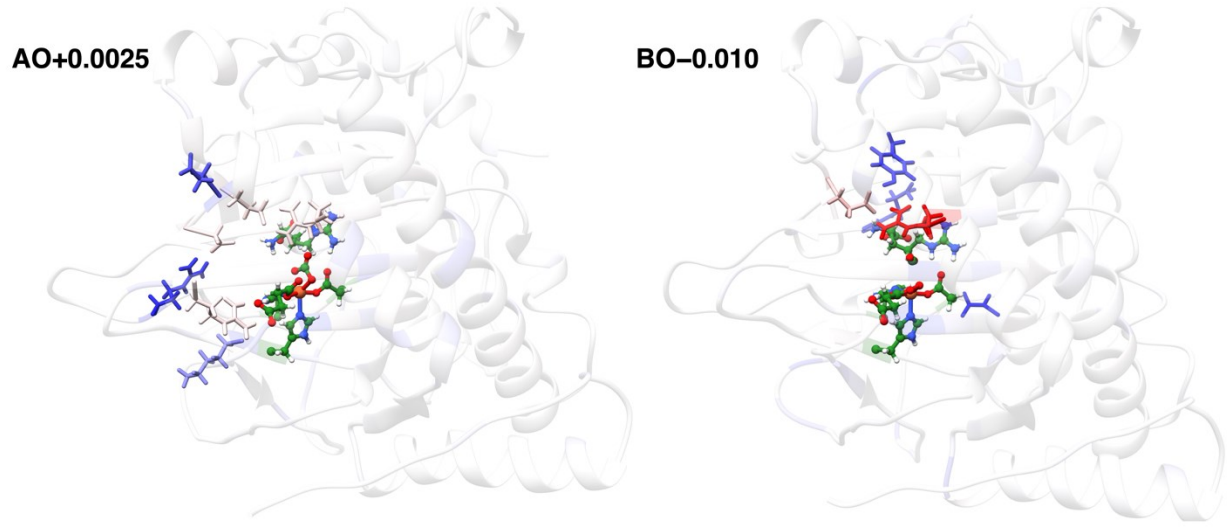

Figure 5. Primary residues stabilizing (blue) and destabilizing (red) the ExtEF-induced Fe(II)-succinyl-peroxy carbonate intermediate (used for ethylene formation) with respect to the RC in

AO+0.0025 and Fe(II)-succinyl-peroxide intermediate (used for L-Arg hydroxylation) with respect to the RC in **BO-0.010**. Darker red and blue colors indicate a higher magnitude of contributions.

The switching from L-Arg hydroxylation to ethylene production in the **AO** snapshot using an ExtEF of +0.0025 au leads to a substantial decrease in the energetic magnitudes of most residues compared to the **AO-noExtEF** (Figures 5, S5). For example, the energetic contribution of E84 reduces from 8.27 to 1.60, D91 reduces from 7.11 to 1.96, R171 reduces from 5.90 to 1.68, and R184 reduces (in absolute value) from -3.59 to -0.84. In contrast, the predicted switch from ethylene production preference towards L-Arg hydroxylation in the **BO** snapshot using -0.010 au ExtEF leads to a sharp increase in the energetic contributions from residues (Figures 5, S6). The R171 and E84 contributions towards destabilizing the intermediate increase to 12.94 and 3.42 in **BO-0.010** compared to -1.31 and 1.79 kcal/mol in **BO-noExtEF**. The magnitudes of the residues contributing to the stabilization of the intermediate are also high in the ExtEF L-Arg hydroxylation intermediate (Figure S4). *Residues R171, E84, and D91 change their contributions in both ExtEF-induced reactivity switches, suggesting that they might play a key role in controlling the EFE reactivity for ethylene formation versus L-Arg hydroxylation. Our study suggests that the ExtEF-led change of the energetic contributions from the SCS residues might be the key factor for switching between the competing reactions of ethylene formation and L-Arg hydroxylation in EFE. In other words, the ExtEF can remove the importance of the L-Arg substrate's conformational state in EFE's reactivities.*

Conclusions

In this study, we suggest that applying an ExtEF along the Fe-O bond of the EFE·Fe(III)·$OO^{\cdot-}$·2OG·L-Arg complex can switch between the competing reactions of ethylene formation or L-Arg hydroxylation. The results indicate that **AO-RC**, associated with L-Arg hydroxylation reactivity,[20] exhibits a more negative IntEF. In contrast, the ethylene-associated **BO-RC**[20] is characterized by a less negative IntEF along the Fe-O bond. We predict that applying a positive ExtEF (i.e., reducing the IntEF of EFE) along the Fe-O bond for the enzyme using an off-line bound 2OG coordination mode will lead to ethylene reaction preference irrespective of the L-Arg conformation. In contrast, an in-line coordinated 2OG in EFE leads to L-Arg hydroxylation for both the L-Arg conformations regardless of the magnitude and the sign of the applied ExtEF.

Additionally, analysis indicates that applying an ExtEF affects the Fe-O bond lengths and their spin densities. Upon application of ExtEFs, the nature of the bonding orbitals and their reactivities are affected. Applying positive ExtEFs leads to the movement of electron density from the dioxygen-based orbital to the Fe-based orbital. An opposite movement of electron density from the Fe-based orbital to the dioxygen-based orbital is detected by applying negative ExtEFs. The EDA results show that the stabilization of the Fe(II)-succinyl-peroxy carbonate intermediate in the ethylene reaction is related to lower magnitudes of energetic contributions from SCS residues. In contrast, the Fe(II)-succinyl-peroxide intermediate during L-Arg hydroxylation requires higher magnitudes of energetic contributions from the SCS residues. R171, E84, and D91 change the magnitude of their energy contributions drastically in the two reactions and might modulate between the ethylene and L-Arg hydroxylation pathways. Importantly site-directed mutagenesis studies where individual residues responsible for stabilizing the key intermediates

in the two reactions of EFE were substituted with alanine led to changes in EFE activity, thus confirming their importance for catalysis.

The overall results further reveal the mechanistic strategy of EFE. It shows that when 2OG is bound in an off-line coordination mode, released CO_2 during the O_2 attack on 2OG can be stabilized by R171 for the C1-C2 bond insertion mechanism.[20] When this steric condition is satisfied, the changes in the IntEF of EFE caused by the substrate L-Arg conformation or by the applied ExtEF can prioritize either ethylene formation or L-Arg hydroxylation reactions. For the in-line 2OG coordination mode, where the CO_2 is not stabilized in the active site,[20] electrostatic changes do not seem to change the preference for the L-Arg hydroxylation reaction. The current study suggests that making the IntEF of EFE less negative and stabilizing the off-line binding of 2OG might increase the ethylene yield. This prediction suggests that the effects of an ExtEF are multidimensional and multifaced - ExtEF polarizes the electronic structure in the QM part of the molecule and also alternates and modulates the individual energy contributions of residues in the SCS and remote regions of the enzyme. The combined effects of the SCS and the QM parts afford synergy that can lead to a switch of reactivities. The results offer a strategy to increase ethylene production by EFE by mimicking the electric field changes that lead to ethylene reactivity via variations of residues in the SCS and beyond. The present study is a proof-of-concept that demonstrates *in silico,* the feasibility of the approach to influence the reactivity of the EFE by applying an ExtEF.

Supporting Information

The QM geometries of QM/MM optimized structures, spin densities, Mulliken charges, supporting data on orbitals, and the EDA results are included in Supporting Information.

Acknowledgments

This research was supported by the NSF grants 1904215, 2203630 to CZC, and 1904295, 2203472 to JH and RPH. We thank Sarah Atkinson for her technical assistance.

References

(1) Fernelius, C. W.; Wittcoff, H.; Varnerin, R. E. Ethylene: The Organic Chemical Industry's Most Important Building Block. *J. Chem. Educ.* **1979**, *56* (6), 385. https://doi.org/10.1021/ed056p385.

(2) Chenier, P. J. Derivatives of Ethylene. In *Survey of Industrial Chemistry*; Chenier, P. J., Ed.; Topics in Applied Chemistry; Springer US: Boston, MA, 2002; pp 143–162. https://doi.org/10.1007/978-1-4615-0603-4_9.

(3) Burg, S. P.; Burg, E. A. Ethylene Action and the Ripening of Fruits. *Science* **1965**, *148* (3674), 1190–1196. https://doi.org/10.1126/science.148.3674.1190.

(4) Ghanta, M.; Fahey, D.; Subramaniam, B. Environmental Impacts of Ethylene Production from Diverse Feedstocks and Energy Sources. *Appl. Petrochem. Res.* **2014**, *4* (2), 167–179. https://doi.org/10.1007/s13203-013-0029-7.

(5) Weingart, H.; Völksch, B.; Ullrich, M. S. Comparison of Ethylene Production by Pseudomonas Syringae and Ralstonia Solanacearum. *Phytopathology®* **1999**, *89* (5), 360–365. https://doi.org/10.1094/PHYTO.1999.89.5.360.

(6) Fukuda, H.; Kitajima, H.; Fujii, T.; Tazaki, M.; Ogawa, T. Purification and Some Properties of a Novel Ethylene-Forming Enzyme Produced by Penicillium Digitatum. *FEMS Microbiol. Lett.* **1989**, *59* (1–2), 1–5. https://doi.org/10.1111/j.1574-6968.1989.tb03072.x.

(7) Martinez, S.; Fellner, M.; Herr, C. Q.; Ritchie, A.; Hu, J.; Hausinger, R. P. Structures and Mechanisms of the Non-Heme Fe(II)- and 2-Oxoglutarate-Dependent Ethylene-Forming Enzyme: Substrate Binding Creates a Twist. *J. Am. Chem. Soc.* **2017**, *139* (34), 11980–11988. https://doi.org/10.1021/jacs.7b06186.

(8) Zhang, Z.; Smart, T. J.; Choi, H.; Hardy, F.; Lohans, C. T.; Abboud, M. I.; Richardson, M. S. W.; Paton, R. S.; McDonough, M. A.; Schofield, C. J. Structural and Stereoelectronic Insights into Oxygenase-Catalyzed Formation of Ethylene from 2-Oxoglutarate. *Proc. Natl. Acad. Sci.* **2017**, *114* (18), 4667–4672. https://doi.org/10.1073/pnas.1617760114.

(9) Li, M.; Martinez, S.; Hausinger, R. P.; Emerson, J. P. Thermodynamics of Iron(II) and Substrate Binding to the Ethylene-Forming Enzyme. *Biochemistry* **2018**, *57* (39), 5696–5705. https://doi.org/10.1021/acs.biochem.8b00730.

(10) Martinez, S.; Hausinger, R. P. Biochemical and Spectroscopic Characterization of the Non-Heme Fe(II)- and 2-Oxoglutarate-Dependent Ethylene-Forming Enzyme from Pseudomonas Syringae Pv. Phaseolicola PK2. *Biochemistry* **2016**, *55* (43), 5989–5999. https://doi.org/10.1021/acs.biochem.6b00890.
(11) Fukuda, H.; Ogawa, T.; Tazaki, M.; Nagahama, K.; Fujiil, T.; Tanase, S.; Morino, Y. Two Reactions Are Simultaneously Catalyzed by a Single Enzyme: The Arginine-Dependent Simultaneous Formation of Two Products, Ethylene and Succinate, from 2-Oxoglutarate by an Enzyme from Pseudomonas Syringae. *Biochem. Biophys. Res. Commun.* **1992**, *188* (2), 483–489. https://doi.org/10.1016/0006-291X(92)91081-Z.
(12) Copeland, R. A.; Davis, K. M.; Shoda, T. K. C.; Blaesi, E. J.; Boal, A. K.; Krebs, C.; Bollinger, J. M. An Iron(IV)–Oxo Intermediate Initiating l-Arginine Oxidation but Not Ethylene Production by the 2-Oxoglutarate-Dependent Oxygenase, Ethylene-Forming Enzyme. *J. Am. Chem. Soc.* **2021**, *143* (5), 2293–2303. https://doi.org/10.1021/jacs.0c10923.
(13) Copeland, R. A.; Zhou, S.; Schaperdoth, I.; Shoda, T. K. C.; Bollinger, J. M.; Krebs, C. Hybrid Radical-Polar Pathway for Excision of Ethylene from 2-Oxoglutarate by an Iron Oxygenase. *Science* **2021**, *373* (6562), 1489–1493. https://doi.org/10.1126/science.abj4290.
(14) Nagahama, K.; Ogawa, T.; Fujii, T.; Tazaki, M.; Tanase, S.; Morino, Y.; Fukuda, H. Purification and Properties of an Ethylene-Forming Enzyme from Pseudomonas Syringae Pv. Phaseolicola PK2. *J. Gen. Microbiol.* **1991**, *137* (10), 2281–2286. https://doi.org/10.1099/00221287-137-10-2281.
(15) Kallio, P.; Kugler, A.; Pyytövaara, S.; Stensjö, K.; Allahverdiyeva, Y.; Gao, X.; Lindblad, P.; Lindberg, P. Photoautotrophic Production of Renewable Ethylene by Engineered Cyanobacteria: Steering the Cell Metabolism towards Biotechnological Use. *Physiol. Plant.* **2021**, *173* (2), 579–590. https://doi.org/10.1111/ppl.13430.
(16) Sengupta, A.; Pritam, P.; Jaiswal, D.; Bandyopadhyay, A.; Pakrasi, H. B.; Wangikar, P. P. Photosynthetic Co-Production of Succinate and Ethylene in a Fast-Growing Cyanobacterium, Synechococcus Elongatus PCC 11801. *Metabolites* **2020**, *10* (6), 250. https://doi.org/10.3390/metabo10060250.
(17) Ducat, D. C.; Way, J. C.; Silver, P. A. Engineering Cyanobacteria to Generate High-Value Products. *Trends Biotechnol.* **2011**, *29* (2), 95–103. https://doi.org/10.1016/j.tibtech.2010.12.003.
(18) Vaud, S.; Pearcy, N.; Hanževački, M.; Van Hagen, A. M. W.; Abdelrazig, S.; Safo, L.; Ehsaan, M.; Jonczyk, M.; Millat, T.; Craig, S.; Spence, E.; Fothergill, J.; Bommareddy, R. R.; Colin, P.-Y.; Twycross, J.; Dalby, P. A.; Minton, N. P.; Jäger, C. M.; Kim, D.-H.; Yu, J.; Maness, P.-C.; Lynch, S.; Eckert, C. A.; Conradie, A.; Bryan, S. J. Engineering Improved Ethylene Production: Leveraging Systems Biology and Adaptive Laboratory Evolution. *Metab. Eng.* **2021**, *67*, 308–320. https://doi.org/10.1016/j.ymben.2021.07.001.
(19) Xue, J.; Lu, J.; Lai, W. Mechanistic Insights into a Non-Heme 2-Oxoglutarate-Dependent Ethylene-Forming Enzyme: Selectivity of Ethylene-Formation *versus* L -Arg Hydroxylation. *Phys. Chem. Chem. Phys.* **2019**, *21* (19), 9957–9968. https://doi.org/10.1039/C9CP00794F.
(20) Chaturvedi, S. S.; Ramanan, R.; Hu, J.; Hausinger, R. P.; Christov, C. Z. Atomic and Electronic Structure Determinants Distinguish between Ethylene Formation and L-Arginine

Hydroxylation Reaction Mechanisms in the Ethylene-Forming Enzyme. *ACS Catal.* **2021**, *11* (3), 1578–1592. https://doi.org/10.1021/acscatal.0c03349.
(21) Yeh, C.-C. G.; Ghafoor, S.; Satpathy, J. K.; Mokkawes, T.; Sastri, C. V.; de Visser, S. P. Cluster Model Study into the Catalytic Mechanism of α-Ketoglutarate Biodegradation by the Ethylene-Forming Enzyme Reveals Structural Differences with Nonheme Iron Hydroxylases. *ACS Catal.* **2022**, *12* (7), 3923–3937. https://doi.org/10.1021/acscatal.1c04029.
(22) *2-Oxoglutarate-Dependent Oxygenases:*; Schofield, C., Hausinger, R., Eds.; Metallobiology; Royal Society of Chemistry: Cambridge, 2015. https://doi.org/10.1039/9781782621959.
(23) Solomon, E. I.; Goudarzi, S.; Sutherlin, K. D. O2 Activation by Non-Heme Iron Enzymes. *Biochemistry* **2016**, *55* (46), 6363–6374. https://doi.org/10.1021/acs.biochem.6b00635.
(24) Mitchell, A. J.; Dunham, N. P.; Martinie, R. J.; Bergman, J. A.; Pollock, C. J.; Hu, K.; Allen, B. D.; Chang, W.; Silakov, A.; Bollinger, J. M.; Krebs, C.; Boal, A. K. Visualizing the Reaction Cycle in an Iron(II)- and 2-(Oxo)-Glutarate-Dependent Hydroxylase. *J. Am. Chem. Soc.* **2017**, *139* (39), 13830–13836. https://doi.org/10.1021/jacs.7b07374.
(25) Johansson, N.; Persson, K. O.; Larsson, C.; Norbeck, J. Comparative Sequence Analysis and Mutagenesis of Ethylene Forming Enzyme (EFE) 2-Oxoglutarate/Fe(II)-Dependent Dioxygenase Homologs. *BMC Biochem.* **2014**, *15* (1), 22. https://doi.org/10.1186/1471-2091-15-22.
(26) Chaturvedi, S. S.; Ramanan, R.; Lehnert, N.; Schofield, C. J.; Karabencheva-Christova, T. G.; Christov, C. Z. Catalysis by the Non-Heme Iron(II) Histone Demethylase PHF8 Involves Iron Center Rearrangement and Conformational Modulation of Substrate Orientation. *ACS Catal.* **2020**, *10* (2), 1195–1209. https://doi.org/10.1021/acscatal.9b04907.
(27) Waheed, S. O.; Ramanan, R.; Chaturvedi, S. S.; Lehnert, N.; Schofield, C. J.; Christov, C. Z.; Karabencheva-Christova, T. G. Role of Structural Dynamics in Selectivity and Mechanism of Non-Heme Fe(II) and 2-Oxoglutarate-Dependent Oxygenases Involved in DNA Repair. *ACS Cent. Sci.* **2020**, *6* (5), 795–814. https://doi.org/10.1021/acscentsci.0c00312.
(28) Ali, H. S.; Visser, S. P. Electrostatic Perturbations in the Substrate-Binding Pocket of Taurine/A-Ketoglutarate Dioxygenase Determine Its Selectivity. *Chem. – Eur. J.* **2022**, *28* (9), e202104167. https://doi.org/10.1002/chem.202104167.
(29) Wojdyla, Z.; Borowski, T. Properties of the Reactants and Their Interactions within and with the Enzyme Binding Cavity Determine Reaction Selectivities. The Case of Fe(II)/2-Oxoglutarate Dependent Enzymes. *Chem. – Eur. J.* **2022**, *28* (18), e202104106. https://doi.org/10.1002/chem.202104106.
(30) de Visser, S. P.; Mukherjee, G.; Ali, H. S.; Sastri, C. V. Local Charge Distributions, Electric Dipole Moments, and Local Electric Fields Influence Reactivity Patterns and Guide Regioselectivities in α-Ketoglutarate-Dependent Non-Heme Iron Dioxygenases. *Acc. Chem. Res.* **2022**, *55* (1), 65–74. https://doi.org/10.1021/acs.accounts.1c00538.
(31) Bím, D.; Alexandrova, A. N. Local Electric Fields As a Natural Switch of Heme-Iron Protein Reactivity. *ACS Catal.* **2021**, *11* (11), 6534–6546. https://doi.org/10.1021/acscatal.1c00687.
(32) Dubey, K. D.; Stuyver, T.; Shaik, S. Local Electric Fields: From Enzyme Catalysis to Synthetic Catalyst Design. *J. Phys. Chem. B* **2022**, *126* (49), 10285–10294. https://doi.org/10.1021/acs.jpcb.2c06422.

(33) Meir, R.; Chen, H.; Lai, W.; Shaik, S. Oriented Electric Fields Accelerate Diels–Alder Reactions and Control the Endo/Exo Selectivity. *ChemPhysChem* **2010**, *11* (1), 301–310. https://doi.org/10.1002/cphc.200900848.
(34) Peng, W.; Yan, S.; Zhang, X.; Liao, L.; Zhang, J.; Shaik, S.; Wang, B. How Do Preorganized Electric Fields Function in Catalytic Cycles? The Case of the Enzyme Tyrosine Hydroxylase. *J. Am. Chem. Soc.* **2022**, *144* (44), 20484–20494. https://doi.org/10.1021/jacs.2c09263.
(35) Fried, S. D. E.; Zheng, C.; Mao, Y.; Markland, T. E.; Boxer, S. G. Solvent Organization and Electrostatics Tuned by Solute Electronic Structure: Amide versus Non-Amide Carbonyls. *J. Phys. Chem. B* **2022**, *126* (31), 5876–5886. https://doi.org/10.1021/acs.jpcb.2c03095.
(36) Hennefarth, M. R.; Alexandrova, A. N. Advances in Optimizing Enzyme Electrostatic Preorganization. *Curr. Opin. Struct. Biol.* **2022**, *72*, 1–8. https://doi.org/10.1016/j.sbi.2021.06.006.
(37) Fried, S. D.; Bagchi, S.; Boxer, S. G. Extreme Electric Fields Power Catalysis in the Active Site of Ketosteroid Isomerase. *Science* **2014**, *346* (6216), 1510–1514. https://doi.org/10.1126/science.1259802.
(38) Shaik, S.; Ramanan, R.; Danovich, D.; Mandal, D. Structure and Reactivity/Selectivity Control by Oriented-External Electric Fields. *Chem. Soc. Rev.* **2018**, *47* (14), 5125–5145. https://doi.org/10.1039/C8CS00354H.
(39) Shaik, S.; Danovich, D.; Joy, J.; Wang, Z.; Stuyver, T. Electric-Field Mediated Chemistry: Uncovering and Exploiting the Potential of (Oriented) Electric Fields to Exert Chemical Catalysis and Reaction Control. *J. Am. Chem. Soc.* **2020**, *142* (29), 12551–12562. https://doi.org/10.1021/jacs.0c05128.
(40) Stuyver, T.; Ramanan, R.; Mallick, D.; Shaik, S. Oriented (Local) Electric Fields Drive the Millionfold Enhancement of the H-Abstraction Catalysis Observed for Synthetic Metalloenzyme Analogues. *Angew. Chem. Int. Ed.* **2020**, *59* (20), 7915–7920. https://doi.org/10.1002/anie.201916592.
(41) Shaik, S.; Mandal, D.; Ramanan, R. Oriented Electric Fields as Future Smart Reagents in Chemistry. *Nat. Chem.* **2016**, *8* (12), 1091–1098. https://doi.org/10.1038/nchem.2651.
(42) Lai, W.; Chen, H.; Cho, K.-B.; Shaik, S. External Electric Field Can Control the Catalytic Cycle of Cytochrome P450cam: A QM/MM Study. *J. Phys. Chem. Lett.* **2010**, *1* (14), 2082–2087. https://doi.org/10.1021/jz100695n.
(43) Meir, R.; Chen, H.; Lai, W.; Shaik, S. Oriented Electric Fields Accelerate Diels–Alder Reactions and Control the *Endo* / *Exo* Selectivity. *ChemPhysChem* **2010**, *11* (1), 301–310. https://doi.org/10.1002/cphc.200900848.
(44) Aragonès, A. C.; Haworth, N. L.; Darwish, N.; Ciampi, S.; Bloomfield, N. J.; Wallace, G. G.; Diez-Perez, I.; Coote, M. L. Electrostatic Catalysis of a Diels–Alder Reaction. *Nature* **2016**, *531* (7592), 88–91. https://doi.org/10.1038/nature16989.
(45) Waheed, S. O.; Chaturvedi, S. S.; Karabencheva-Christova, T. G.; Christov, C. Z. Catalytic Mechanism of Human Ten-Eleven Translocation-2 (TET2) Enzyme: Effects of Conformational Changes, Electric Field, and Mutations. *ACS Catal.* **2021**, *11* (7), 3877–3890. https://doi.org/10.1021/acscatal.0c05034.
(46) Ramanan, R.; Waheed, S. O.; Schofield, C. J.; Christov, C. Z. What Is the Catalytic Mechanism of Enzymatic Histone N-Methyl Arginine Demethylation and Can It Be

Influenced by an External Electric Field? *Chem. – Eur. J.* **2021**, *27* (46), 11827–11836. https://doi.org/10.1002/chem.202101174.
(47) Shaik, S.; de Visser, S. P.; Kumar, D. External Electric Field Will Control the Selectivity of Enzymatic-Like Bond Activations. *J. Am. Chem. Soc.* **2004**, *126* (37), 11746–11749. https://doi.org/10.1021/ja047432k.
(48) Wang, C.; Danovich, D.; Chen, H.; Shaik, S. Oriented External Electric Fields: Tweezers and Catalysts for Reactivity in Halogen-Bond Complexes. *J. Am. Chem. Soc.* **2019**, *141* (17), 7122–7136. https://doi.org/10.1021/jacs.9b02174.
(49) Stuyver, T.; Danovich, D.; Joy, J.; Shaik, S. External Electric Field Effects on Chemical Structure and Reactivity. *WIREs Comput. Mol. Sci.* **2020**, *10* (2), e1438. https://doi.org/10.1002/wcms.1438.
(50) Siddiqui, S. A.; Dubey, K. D. Can the Local Electric Field Be a Descriptor of Catalytic Activity? A Case Study on Chorismate Mutase. *Phys. Chem. Chem. Phys.* **2022**, *24* (4), 1974–1981. https://doi.org/10.1039/D1CP03978D.
(51) Che, F.; Gray, J. T.; Ha, S.; Kruse, N.; Scott, S. L.; McEwen, J.-S. Elucidating the Roles of Electric Fields in Catalysis: A Perspective. *ACS Catal.* **2018**, *8* (6), 5153–5174. https://doi.org/10.1021/acscatal.7b02899.
(52) Berman, H. M.; Westbrook, J.; Feng, Z.; Gilliland, G.; Bhat, T. N.; Weissig, H.; Shindyalov, I. N.; Bourne, P. E. The Protein Data Bank. *Nucleic Acids Res.* **2000**, *28* (1), 235–242. https://doi.org/10.1093/nar/28.1.235.
(53) GaussView, Version 6.1.1, Roy Dennington, Todd Keith, and John Millam, Semichem Inc., Shawnee Mission, KS, 2019.
(54) Pettersen, E. F.; Goddard, T. D.; Huang, C. C.; Couch, G. S.; Greenblatt, D. M.; Meng, E. C.; Ferrin, T. E. UCSF Chimera--a Visualization System for Exploratory Research and Analysis. *J. Comput. Chem.* **2004**, *25* (13), 1605–1612. https://doi.org/10.1002/jcc.20084.
(55) Wang, J.; Wang, W.; Kollman, P. A.; Case, D. A. Automatic atom type and bond type perception in molecular mechanical calculations. *J Mol Graph Model* **2006**, *25* (2), 247–260.
(56) Li, P.; Merz, K. M. MCPB.Py: A Python Based Metal Center Parameter Builder. *J. Chem. Inf. Model.* **2016**, *56* (4), 599–604. https://doi.org/10.1021/acs.jcim.5b00674.
(57) Maier, J. A.; Martinez, C.; Kasavajhala, K.; Wickstrom, L.; Hauser, K. E.; Simmerling, C. Ff14SB: Improving the Accuracy of Protein Side Chain and Backbone Parameters from Ff99SB. *J. Chem. Theory Comput.* **2015**, *11* (8), 3696–3713. https://doi.org/10.1021/acs.jctc.5b00255.
(58) D.A. Case, R.M. Betz, D.S. Cerutti, T.E. Cheatham, III, T.A. Darden, R.E. Duke, T.J. Giese, H. Gohlke, A.W. Goetz, N. Homeyer, S. Izadi, P. Janowski, J. Kaus, A. Kovalenko, T.S. Lee, S. LeGrand, P. Li, C. Lin, T. Luchko, R. Luo, B. Madej, D. Mermelstein, K.M. Merz, G. Monard, H. Nguyen, H.T. Nguyen, I. Omelyan, A. Onufriev, D.R. Roe, A. Roitberg, C. Sagui, C.L. Simmerling, W.M. Botello-Smith, J. Swails, R.C. Walker, J. Wang, R.M. Wolf, X. Wu, L. Xiao and P.A. Kollman (2016), AMBER 2016, University of California, San Francisco.
(59) Davidchack et al. - 2009 - Langevin Thermostat for Rigid Body Dynamics.
(60) Berendsen, H. J. C.; Postma, J. P. M.; Gunsteren, W. F.; Dinola, A.; Haak, J. Molecular Dynamics with Coupling to an External Bath. *J Chem Phys* **1984**, *81* (8), 3684–3690.

(61) Ryckaert, J.-P.; Ciccotti, G.; Berendsen, H. J. C. Numerical Integration of the Cartesian Equations of Motion of a System with Constraints: Molecular Dynamics of n-Alkanes. *J. Comput. Phys.* **1977**, *23* (3), 327–341. https://doi.org/10.1016/0021-9991(77)90098-5.
(62) Darden, T.; York, D.; Pedersen, L. Particle Mesh Ewald: An N·log(N) Method for Ewald Sums in Large Systems. *J Chem Phys* **1993**, *98* (12), 10089–10092.
(63) Stuyver, T.; Huang, J.; Mallick, D.; Danovich, D.; Shaik, S. TITAN: A Code for Modeling and Generating Electric Fields—Features and Applications to Enzymatic Reactivity. *J. Comput. Chem.* **2020**, *41* (1), 74–82. https://doi.org/10.1002/jcc.26072.
(64) Metz, S.; Kästner, J.; Sokol, A. A.; Keal, T. W.; Sherwood, P. ChemShell—a Modular Software Package for QM/MM Simulations. *WIREs Comput. Mol. Sci.* **2014**, *4* (2), 101–110. https://doi.org/10.1002/wcms.1163.
(65) Ahlrichs, R.; Bär, M.; Häser, M.; Horn, H.; Kölmel, C. Electronic Structure Calculations on Workstation Computers: The Program System Turbomole. *Chem. Phys. Lett.* **1989**, *162* (3), 165–169. https://doi.org/10.1016/0009-2614(89)85118-8.
(66) Smith, W.; Yong, C. W.; Rodger, P. M. DL_POLY: Application to Molecular Simulation. *Mol. Simul.* **2002**, *28* (5), 385–471. https://doi.org/10.1080/08927020290018769.
(67) Solomon, E. I.; Light, K. M.; Liu, L. V.; Srnec, M.; Wong, S. D. Geometric and Electronic Structure Contributions to Function in Non-Heme Iron Enzymes. *Acc. Chem. Res.* **2013**, *46* (11), 2725–2739. https://doi.org/10.1021/ar400149m.
(68) Becke, A. D. Density-functional Thermochemistry. III. The Role of Exact Exchange. *J. Chem. Phys.* **1993**, *98* (7), 5648–5652. https://doi.org/10.1063/1.464913.
(69) Ramanan, R.; Chaturvedi, S. S.; Lehnert, N.; Schofield, C. J.; Karabencheva-Christova, T. G.; Christov, C. Z. Catalysis by the JmjC Histone Demethylase KDM4A Integrates Substrate Dynamics, Correlated Motions and Molecular Orbital Control. *Chem. Sci.* **2020**, *11* (36), 9950–9961. https://doi.org/10.1039/D0SC03713C.
(70) Álvarez-Barcia, S.; Kästner, J. Atom Tunneling in the Hydroxylation Process of Taurine/α-Ketoglutarate Dioxygenase Identified by Quantum Mechanics/Molecular Mechanics Simulations. *J. Phys. Chem. B* **2017**, *121* (21), 5347–5354. https://doi.org/10.1021/acs.jpcb.7b03477.
(71) Ye, S.; Riplinger, C.; Hansen, A.; Krebs, C.; Bollinger Jr., J. M.; Neese, F. Electronic Structure Analysis of the Oxygen-Activation Mechanism by FeII- and α-Ketoglutarate (AKG)-Dependent Dioxygenases. *Chem. – Eur. J.* **2012**, *18* (21), 6555–6567. https://doi.org/10.1002/chem.201102829.
(72) Waheed, S. O.; Varghese, A.; Chaturvedi, S. S.; Karabencheva-Christova, T. G.; Christov, C. Z. How Human TET2 Enzyme Catalyzes the Oxidation of Unnatural Cytosine Modifications in Double-Stranded DNA. *ACS Catal.* **2022**, 5327–5344. https://doi.org/10.1021/acscatal.2c00024.
(73) Calixto, A. R.; Ramos, M. J.; Fernandes, P. A. Influence of Frozen Residues on the Exploration of the PES of Enzyme Reaction Mechanisms. *J. Chem. Theory Comput.* **2017**, *13* (11), 5486–5495. https://doi.org/10.1021/acs.jctc.7b00768.
(74) Bakowies, D.; Thiel, W. Hybrid Models for Combined Quantum Mechanical and Molecular Mechanical Approaches. *J. Phys. Chem.* **1996**, *100* (25), 10580–10594. https://doi.org/10.1021/jp9536514.

(75) Weigend, F.; Ahlrichs, R. Balanced Basis Sets of Split Valence, Triple Zeta Valence and Quadruple Zeta Valence Quality for H to Rn: Design and Assessment of Accuracy. *Phys. Chem. Chem. Phys.* **2005**, *7* (18), 3297. https://doi.org/10.1039/b508541a.
(76) Kästner, J.; Carr, J. M.; Keal, T. W.; Thiel, W.; Wander, A.; Sherwood, P. DL-FIND: An Open-Source Geometry Optimizer for Atomistic Simulations. *J. Phys. Chem. A* **2009**, *113* (43), 11856–11865. https://doi.org/10.1021/jp9028968.
(77) Cisneros, G. A.; Perera, L.; Schaaper, R. M.; Pedersen, L. C.; London, R. E.; Pedersen, L. G.; Darden, T. A. Reaction Mechanism of the ε Subunit of *E. Coli* DNA Polymerase III: Insights into Active Site Metal Coordination and Catalytically Significant Residues. *J. Am. Chem. Soc.* **2009**, *131* (4), 1550–1556. https://doi.org/10.1021/ja8082818.
(78) Graham, S. E.; Syeda, F.; Cisneros, G. A. Computational Prediction of Residues Involved in Fidelity Checking for DNA Synthesis in DNA Polymerase I. *Biochemistry* **2012**, *51* (12), 2569–2578. https://doi.org/10.1021/bi201856m.
(79) Liu, H.; Llano, J.; Gauld, J. W. A DFT Study of Nucleobase Dealkylation by the DNA Repair Enzyme AlkB. *J. Phys. Chem. B* **2009**, *113* (14), 4887–4898. https://doi.org/10.1021/jp810715t.
(80) Wójcik, A.; Radoń, M.; Borowski, T. Mechanism of O_2 Activation by α-Ketoglutarate Dependent Oxygenases Revisited. A Quantum Chemical Study. *J. Phys. Chem. A* **2016**, *120* (8), 1261–1274. https://doi.org/10.1021/acs.jpca.5b12311.

TOC: